ACS OMEGA

http://pubs.acs.org/journal/acsodf

Article

Stabilization and Reinforcement Effect of Fibers on a Bitumen Binder

Mengmeng Wu, Hongmei Cai, Hao Wang, Jia wei Hua, Jilei Liang,* and Yuzhen Zhang

Cite This: *ACS Omega* 2022, 7, 44207−44214

Read Online

ACCESS | Metrics & More | Article Recommendations

ABSTRACT: This study investigated fibers' stabilization and reinforcement effect on a bitumen binder. The fibers' microstructures were primarily observed using scanning electron microscopy, and laboratory tests, including the oven heating and mesh-basket draindown, were designed and carried out on three different fiber−bitumen binders (lignin, mineral, and carbon fiber) in this paper to evaluate the bitumen adsorption and thermal stability, respectively. Then, the cone sink experiment was performed to check the rheological properties of these fiber−bitumen binders. These results reveal that the stabilization and reinforcement effect increases with the fiber content increasing to the optimal value. The optimal fiber content depends on the performance of the fiber−bitumen binder, and the value found in this paper is 0.4 wt %. The results indicate that the fiber enhances the toughness of the bitumen effectively via its spatial framework, adhesion, and stabilization of the fiber−bitumen binder. The rheological properties and rutting resistance were tested by a dynamic shear rheometer, and the results suggested that the fiber could effectively enhance the flow resistance and the rutting resistance of the fiber−bitumen binder.

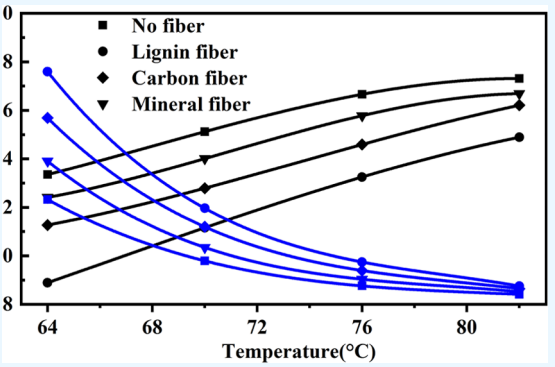

1. INTRODUCTION

For road pavement, the bitumen is subjected to not only high temperature but also severe sun radiation, oxygen, and even other radicals that can accelerate the ageing of the bitumen. Hence, the durability of the bitumen is very important. To improve the performance of the bitumen, many different additives have been added to it, such as polymers, fibers, and nanomaterials. Goshtasp et al. introduced a new nanocomposite bitumen binder, which was modified by clay/fumed silica nanoparticles.[1−3] The new binder showed higher mechanical, chemical, and thermal improvements than the conventional bitumen. In addition, the results indicated that the composite can significantly disrupt chemical oxidation and decomposition and delay aging. Meanwhile, fiber is also a good additive. The addition of different fibers to bitumen, that is to say, the fiber−bitumen binder, is a relatively novel concept in bitumen pavement engineering, even though some early applications with fibers have been introduced.[4,5] Previously, the application of fibers as building materials in lightweight structures and cement concrete was recognized over 50 years ago.[6,7] Recent surveys show the application of fibers in porous bitumen and stone matrix bitumen is very popular in Western countries.[8,9] For example, three fibers, including the organic fiber, the mineral fiber, and the polyester fiber, have been introduced to the bitumen to stabilize it and cut down the draining of the bitumen.[10,11]

As the matrix material in such a fiber−bitumen binder, bitumen could be strengthened by fibers.[12,13] Conventionally, fibers are used to prevent the matrix bitumen from a draindown when the binder is hot. The binder consisting of the fiber and bitumen may be recognized as the medium bonding the aggregates together. Therefore, the binder is an essential part of the bitumen concrete. Many studies reported that fibers can enhance the anticracking properties at low temperatures, durability, and even the fatigue life of bitumen concrete mixtures.[14,15] Furthermore, fibers could improve material tensile strength,[16,17] dynamic modulus,[18] and elasticity as well as the wear resistance of pavement wearing course.[19] However, the introduction of fibers raises the air voids in the bitumen concrete mixture; as a result, more compaction efforts are required to obtain the same density as that without fibers.[20]

It is well known that the mechanism of the bitumen interacting with fibers is complicated, but the effect on pavement performance is significant. However, a few studies have been performed to explore the reinforcement mechanism

Received: September 2, 2022
Accepted: November 8, 2022
Published: November 18, 2022

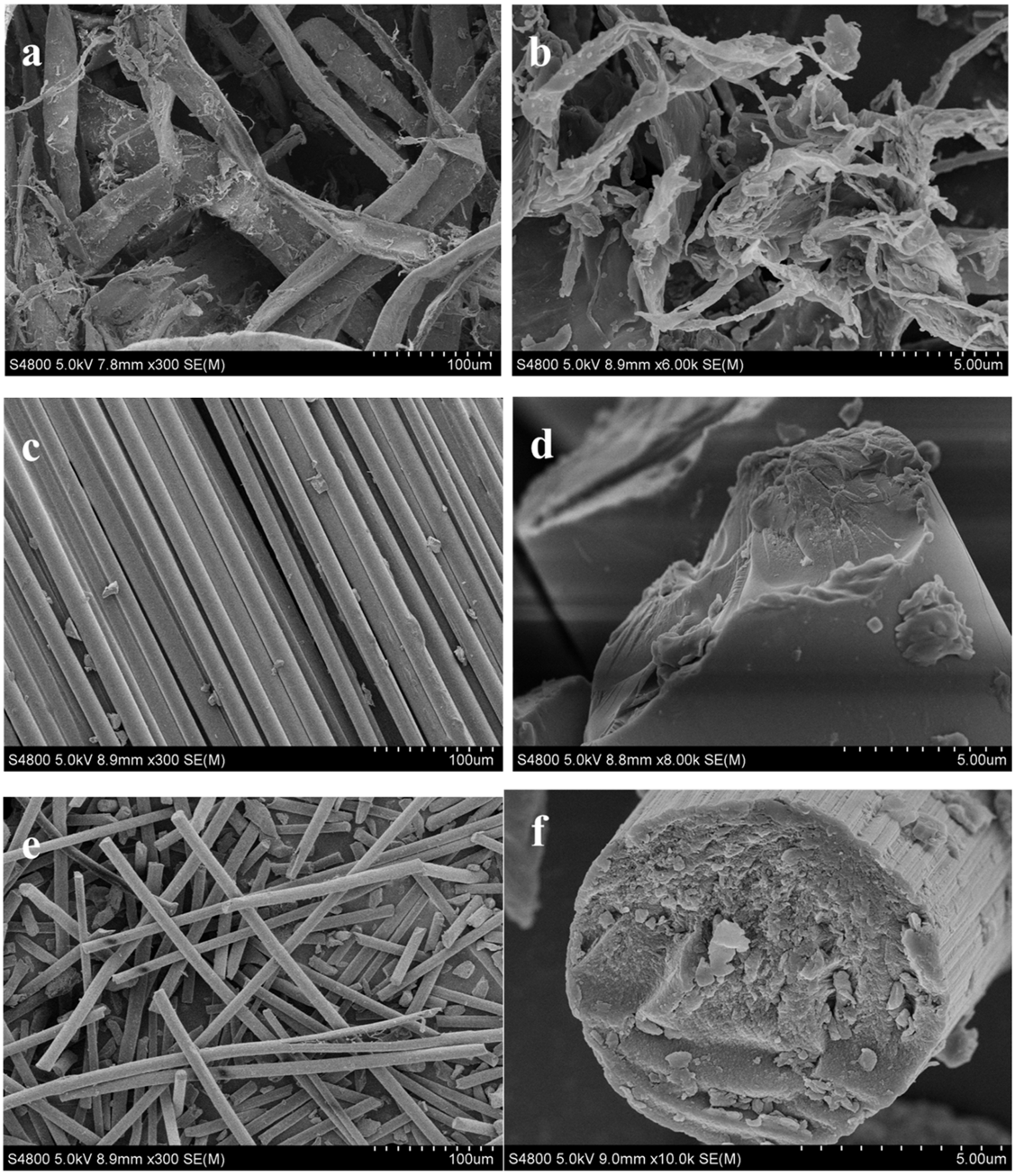

Figure 1. SEM images of fiber microstructures: (a, b) lignin fiber, (c, d) mineral fiber, and (e, f) carbon fiber.

of fibers, especially on the basis of the physical property and microstructure of fibers. Moreover, although fibers could reinforce the fiber−bitumen binder, the optimal content of the fiber is unknown for different fiber−bitumen binders. Consequently, the scanning electron microscopy (SEM), softening point and penetration test, mesh-basket draindown test, cone sink experiment, rheological measurement, and the viscosity of fiber−bitumen binders were studied in this paper to find the stabilization and reinforcement mechanism of different fibers and the optimal fiber contents in different fiber−bitumen binders. The understanding of the properties of the fiber−bitumen binders helps to improve the pavement performance and sheds light on the rational design and preparation of the open-graded friction course fiber−bitumen mixture.

2. RESULTS AND DISCUSSION

2.1. Microstructures of Fibers. Figure 1 displays the SEM images of different fiber microstructures. The lignin fiber shows a distinct loose and porous surface structure. In contrast, the mineral fiber and the carbon fiber demonstrate a much smoother structure. Therefore, the lignin fiber has the largest surface area and the roughest texture among these three fibers, while the mineral fiber possesses the smoothest texture. As shown in Table 4, the surface area of lignin fiber (1.8 m^2/g) is more than 10 times higher than those of the carbon fiber (0.2 m^2/g) and the mineral fiber (0.1 m^2/g). More importantly, the microstructures in the SEM images of the carbon and the mineral fiber are obviously different from that of the lignin fiber, and the former two fibers possess circular cross sections, with relatively smoother textures and smaller surface areas. The

https://doi.org/10.1021/acsomega.2c05677
ACS Omega 2022, 7, 44207−44214

surface property can explain the higher capacity of the lignin fiber in binding the bitumen. Papirer et al. reported that the resistance to rutting of the bitumen mixture pavement at high temperatures can be enhanced with the introduction of fibers.[21] The following reasons can account for this phenomenon. Fibers dispersed in the bitumen can absorb the binder on the surface to generate a monolayer, which results in a strong cohesion between the "fiber–bitumen" interlayer and the interlinked framework. The framework cannot collapse at higher temperatures, which leads to a thick binder coating with no drainage of the bitumen. Meanwhile, the light components in the bitumen can also be absorbed by fibers, which can increase the fiber–bitumen binder viscosity. As a result, fibers improve the shear strength of the asphalt binder. Moreover, the higher tensile strength of fibers may accommodate more asphalts and prevent them from flowing and propagation of cracks more efficiently.[22]

2.2. Softening Point and Penetration Results. The softening point (ring and ball test, denoted as T_{r+b}) is also a significant performance criterion for the fiber–bitumen binder. As shown in Figure 2, T_{r+b} increases sharply with the

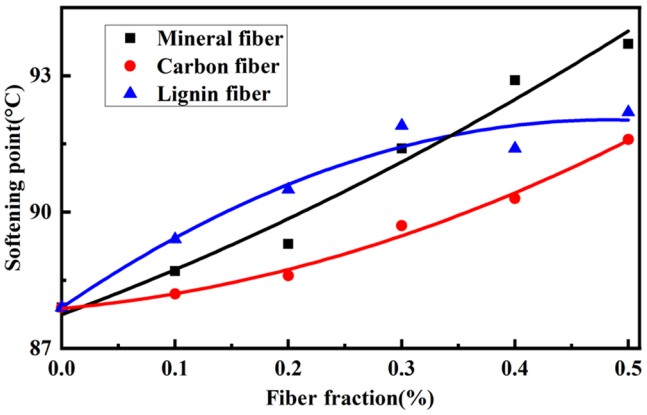

Figure 2. T_{r+b} of different fiber–bitumen binders.

introduction of the fiber. The maximum temperature in the pavement practice can reach 60 °C in summer, and the fiber can help the fiber–bitumen binder to improve its resistance to high temperatures. The fiber content determined by T_{r+b} acts as the minimum value to meet the rainy climate in south China.

The lignin fiber–bitumen binder is inclined to possess a higher T_{r+b} than those containing 0.3 wt % carbon/mineral fiber. Beyond the fiber content, the mineral fiber–bitumen binder demonstrates the highest T_{r+b}. Similar conclusions are drawn from the penetration experiment as well, as presented in Figure 3, which confirms the entanglement effect of the lignin fiber evidently. Although the lignin fiber and the carbon fiber used in this paper are of similar lengths, these two fiber–bitumen binders possess totally different T_{r+b} and penetrations. The reason is that the carbon fiber is not inclined to entangle with each other; however, a similar change in property may be achieved through the introduction of inert fillers to the binder.[23,24]

2.3. Adsorption and Adhesion of Bitumen. Bitumen is made up of asphaltene, aromatic fraction, saturation fraction (paraffins and naphthenes), and resin.[25,26] The fiber can adsorb the components in the bitumen, which changes the rheological properties of the fiber–bitumen binder. Therefore,

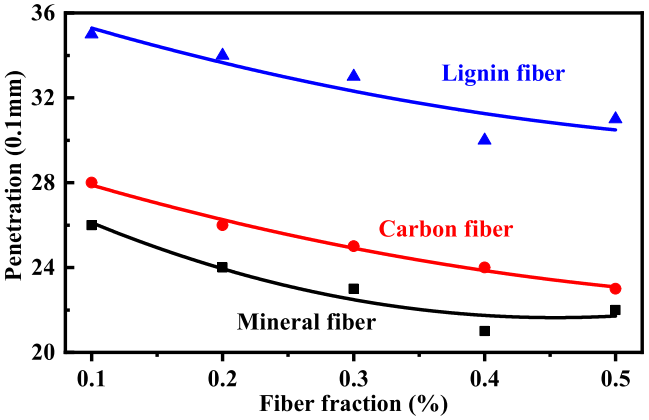

Figure 3. Penetration of different fiber–bitumen binders.

an optimal content of the fiber is required in the design of the fiber–bitumen binder, which is significant in the generation of the interfacial adhesion between the bitumen and the fiber.[23] The mesh-basket draindown experiment was carried out to check the adsorption and stabilization of fibers in the fiber–bitumen binder. Based on the pavement practice, 10 wt % of the fiber in the fiber–bitumen binder was selected. Table 1

Table 1. Results of the Mesh-Basket Draindown Experiment (Bitumen Separation, %)

		bitumen separation (%)			
temperature (°C)	fiber–bitumen binder	30 s	60 s	90 s	120 s
130	carbon fiber	3.12	7.07	8.29	9.14
	mineral fiber	1.34	4.25	5.41	5.99
	lignin fiber	0.00	0.00	0.00	0.00
140	carbon fiber	10.86	12.32	12.78	13.73
	mineral fiber	6.98	7.68	7.92	8.51
	lignin fiber	0.00	0.00	0.00	0.00
170	carbon fiber	15.57	17.87	19.35	20.36
	mineral fiber	9.93	10.85	11.30	11.95
	lignin fiber	0.00	0.05	0.09	0.60

shows the mesh-basket draindown experiment results, and the lignin fiber–bitumen binder has the least separation and drop of bitumen, in other words, the most stabilization and adsorption of the bitumen, followed by the mineral fiber–bitumen binder and the carbon fiber–bitumen binder. The different surface areas and lengths of the two fibers can primarily account for the phenomenon. Compared to the lignin fiber–bitumen binder, the mineral fiber–bitumen binder presents much lower stabilization and adsorption effects on the bitumen, and the reason lies in its smooth surface with lubrication, which can reduce the immersion effect.[27,28]

2.4. Cone Sink Experiment Results. According to the force balance, the shear stress τ (kPa) of different fiber–bitumen binders in the direction tangential to the cone surface was calculated using eq 1,[29] which was used to evaluate the resistance of different fiber–bitumen binders to the flow and shear force.

$$\tau = [G\cdot\cos^2(\alpha/2)]/[\pi\cdot h^2\cdot\tan(\alpha/2)] \quad (1)$$

Here, G is the gravity of the cone (1.025 kN), α is the cone angle (30°), and h is the sink depth (m). Three duplicated samples were tested for different fiber–bitumen binders. Table

https://doi.org/10.1021/acsomega.2c05677
ACS Omega 2022, 7, 44207−44214

2 shows the sink depth h and the shear stress τ of different fiber−bitumen binders, and the results indicated that all fibers

Table 2. Cone Sink Depth h and Shear Stress τ of Different Fiber−Bitumen Binders

items	blank bitumen	carbon fiber	mineral fiber	lignin fiber
fiber fraction (wt %)	0	0.4	0.4	0.4
h (mm)	2.90	2.10	2.70	2.30
τ (MPa)	135.17	257.78	155.94	214.90

can decrease the sink depth h to different extents but increase the shear stress τ. The cone sink depth h of different fiber−bitumen binders is ranked in descending order as follows: the mineral fiber−bitumen binder, the lignin fiber−bitumen binder, and the carbon fiber−bitumen binder.

Two reasons are found to account for the above results. First, the three-dimensional spatial network of fiber can wrap the bitumen tightly. Second, the fiber in the fiber−bitumen binder absorbs the light components in asphalt, resulting in a viscosity increase of the asphalt binder. Consequently, the addition of fiber improves the shear strength of the asphalt binder. Among these fibers, the carbon fiber has the most profound effect on decreasing the cone sink depth h and increasing the shear stress τ of the fiber−bitumen binder, which is owing to its strong internetworking effect. Although the carbon fiber is thick and possesses a smaller surface area, it still shows a better stabilization effect on the bitumen and a stronger interface adhesion. The phenomenon can be interpreted as the solubility law, since the carbon fiber used in this paper originates from the bitumen. In addition, the fiber provides bridging cracking and toughening effects to reinforce the spatial framework; usually, the fiber with a higher tensile strength accommodates the bitumen more efficiently and prevents them from flowing and propagation of cracking.[30,31] Finally, the lignin fiber−bitumen binder possesses a smaller cone sink depth h than that of the mineral fiber−bitumen binder, and the reason lies in its bigger surface area and more adsorption of the bitumen, which can increase the stiffness and viscosity of the fiber−bitumen binder.

2.5. Viscosity Results. The viscosity of the fiber−bitumen binder increases with the lignin fiber content increasing, as shown in Figure 4. With the lignin fiber content of 0.1 wt %, only a slight increase is found in viscosity, which is due to the dispersing material of the lignin fiber. However, as the lignin fiber content increases to 0.3 wt %, the viscosity of the fiber−bitumen binder increases sharply, about 2 to 3 times. The reason is at this content the lignin fiber starts to produce a partial framework structure.[6] As the lignin fiber content continues to increase to 0.4 wt %, the partial framework slowly interacts to form a consecutive framework through the bitumen, leading to a great increase in the viscosity of the fiber−bitumen binder. The consecutive framework plays the part of a supporting structure, which strengthens the fiber−bitumen binder and resists potential deformation.

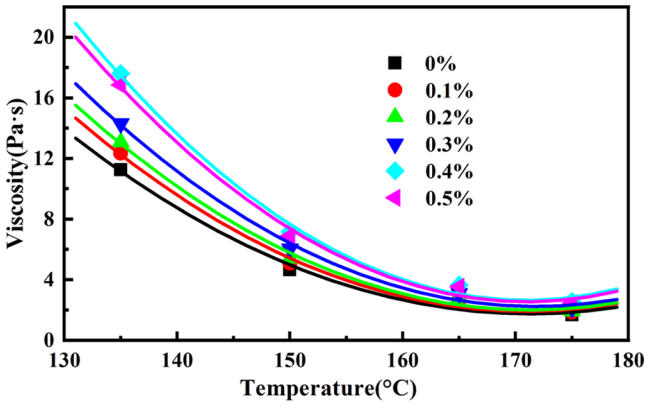

Figure 4. Viscosities of the lignin fiber−bitumen binders with different fiber contents.

The viscosities of different fiber−bitumen binders are presented in Figure 5. At the fiber content of 0.4 wt %, the viscosity of the fiber−bitumen binder begins to present a significant increase. Therefore, the fiber content of 0.4 wt % is the desirable content for the fiber−bitumen binder in view of the reinforcement criterion. Remarkably, the reinforcement effect is one of the most important factors in the determination of the optimal fiber content, and other factors including the fiber−fiber interaction and the construction cost also should be considered. The fiber−bitumen binder containing more fibers than the optimal content brings about not only economic infeasibility but also poor pavement performance. The reason is that the excessive reinforcement of the fiber can produce brittle fiber−bitumen binders, which can deteriorate the pavement performance.[32] Considering that the fiber size has an effect on the viscosity of the fiber−bitumen binder and the longer fiber results in more increase in viscosity, we selected the longer fiber in this paper to obtain the expected viscosity increase. However, the longer fiber may result in mixing problems, which should be paid special attention to.

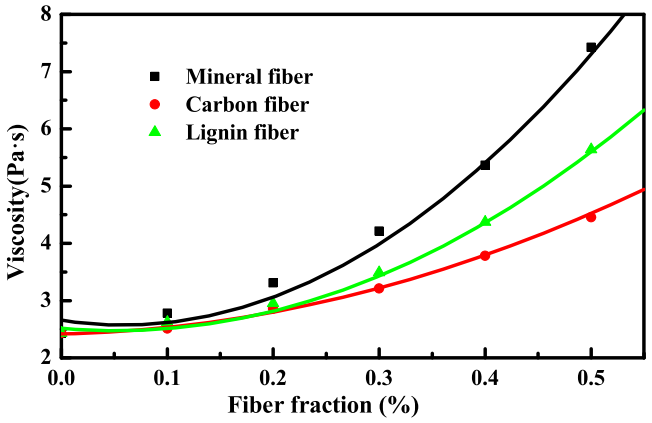

Figure 5. Viscosities of different fiber−bitumen binders at 165 °C.

2.6. Viscoelastic Behavior. To find the effect of the fiber on the rheological properties of the asphalt binder at high temperatures, the dynamic shear rheometer (DSR) experiment was performed with the fiber fraction of 0.4 wt %, and the results are presented in Figure 6. It can be seen that all phase angles δ of both blank bitumen and fiber−bitumen binder are higher than 78° at temperatures of 64−82 °C, indicating the dominance of the viscous composition in both of them. Compared with the phase angles δ of the bitumen, those of the fiber−bitumen binder decreases with the introduction of the fiber, indicating a decrease of the viscous composition but an increase of the elastic composition, which is mainly due to the increase of the modulus brought by the fiber. Meanwhile, the phase angle δ of the fiber−bitumen binder increases linearly

https://doi.org/10.1021/acsomega.2c05677
ACS Omega 2022, 7, 44207−44214

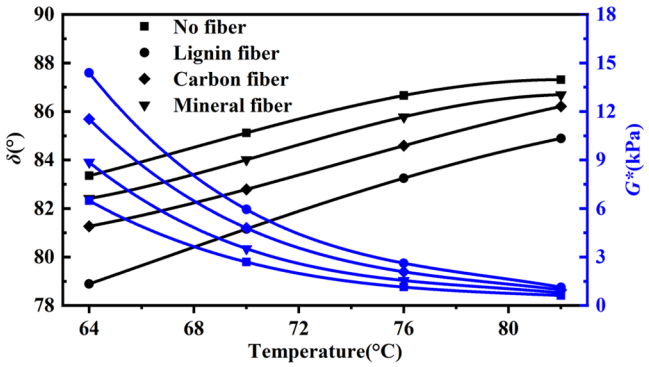

Figure 6. Complex shear modulus (G^*) and phase angle (δ) of different fiber−bitumen binders.

with the increase of temperature, indicating that the viscous composition increases while the elastic composition decreases with the increase of temperature. After the introduction of the fiber, the phase angles δ of all of the fiber−bitumen binders show a similar tendency.

In view of the reasonable ratio of viscous composition and elastic composition, the temperature of the fiber−bitumen binder should not be too low, otherwise, the phase angle δ will decrease. If it is lower than 45°, it easily causes insufficient viscous composition and results in poor fluidity of the bitumen, which may weaken the adhesion of the bitumen to the aggregate. In this paper, at the lowest temperature of 64 °C, the phase angles δ of all of the fiber−bitumen binders are higher than 45°, indicating a reasonable ratio of the viscous composition and the elastic composition and strong adhesion of asphalt to aggregate in these fiber−bitumen binders.

The physical properties of fiber−bitumen binders are different due to the different surface microstructures of fibers. The fiber−bitumen binder is regarded as an organic−inorganic composite, and the difference can also be found in rheology. Figure 7 shows the effect of different fibers on the rheological

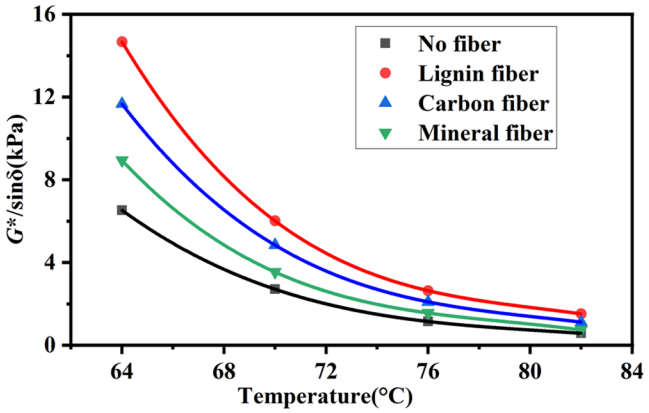

Figure 7. Rutting factors of different fiber−bitumen binders.

properties of fiber−bitumen binders. Compared with those of the blank bitumen (no fiber), Figures 6 and 7 show that rutting factors increase while the phase angles δ decrease of different fiber−bitumen binders, indicating the improvement of high-temperature stability with the addition of the fiber. However, different fibers present different improvements in the rheological properties at high temperatures. For example, at the temperature of 64 °C, the rutting factors of the fiber−bitumen binders with the lignin fiber, the carbon fiber, and the mineral fiber increase by 8.14, 5.14, and 2.41 kPa, respectively, compared with that of the blank bitumen. The results indicate that the lignin fiber−bitumen binder shows the most obvious improvement in the high-temperature rutting resistance, followed by the carbon fiber−bitumen binder and the mineral fiber−bitumen binder. Meanwhile, with the addition of the fibers, the phase angles δ of the fiber−bitumen binders decrease by 4.5, 2.1, and 0.9° for that with the lignin fiber, the carbon fiber, and the mineral fiber, respectively. The result suggests that the lignin fiber has the most evident effect on the increase of elastic components in the fiber−bitumen binder, while the mineral fiber enhances the rheological property of the fiber−bitumen binder at a high temperature via its tackifying effect to some extent.

3. CONCLUSIONS

Fibers can form a spatial framework in the fiber−bitumen binder, and they can reinforce the fiber−bitumen binder by their function of the spatial framework, adsorption, and adhesion of the bitumen. In addition, the microstructure of the fiber can also play an important part in the reinforcement effect. The lignin fiber possesses higher bitumen adsorption than the carbon fiber and the mineral fiber because of the higher surface area. Considering the performance of the fiber−bitumen binder, we selected the optimal fiber content of 0.4 wt % by bitumen concrete weight. The DSR tests showed that fiber−bitumen binders present a greater complex shear modulus G^*, rutting factor $G^*/\sin\delta$, and a smaller phase angle δ compared with the blank bitumen used in the manuscript. Consequently, it is noted that fibers can sharply improve the fiber−bitumen binder flowing resistance and rutting resistance, and the lignin fiber is more suitable for bitumen modification. In view of the engineering practice, mechanical properties including the freeze−thaw split test, immersed Marshall test, and high-temperature rutting test will be performed in the next paper.

4. EXPERIMENTAL SECTION

4.1. Experimental Materials. *4.1.1. Bitumen.* The modified bitumen with high viscosity produced by China Petroleum was used in this paper. To find the basic physical properties of the modified bitumen, some traditional tests such as ductility, softening point, and penetration experiments were performed, and the results are presented in Table 3. Among

Table 3. Physical Properties of Bitumen

items	unit	result	specification
penetration at 25 °C	0.1 mm	62	T0604-2011
ductility at 5 °C	cm	37	T0605-2011
ductility at 10 °C	cm	58	T0605-2011
T_{r+b}	°C	84.5	T0606-2011
viscosity at 60 °C	Pa·s	90,900	T0620-2000
viscosity at 135 °C	Pa·s	1.963	T0625-2011

these tests, the penetration experiment has been performed at 25 °C according to the Specification T0604-2011. The T_{r+b} has been tested according to the Specification T0606-2011, and the ductility has been tested at 5 °C/10 °C according to the Specification T0605-2011.

4.1.2. Fibers. Three different fibers including the wool-like carbon fiber, the loose lignin fiber, and the smooth mineral

https://doi.org/10.1021/acsomega.2c05677
ACS Omega 2022, 7, 44207−44214

fiber acted as stabilizers and were introduced to the modified bitumen. These fibers were predominantly adopted to prevent the fiber−bitumen binder from draindown, especially for the stone matrix bitumen and the porous bitumen in the process of blending, transportation, and compaction. The physical properties of the three fibers were tested and the results are presented in Table 4.

Table 4. Physical Properties of Fibers (Provided by Manufactures)

items	carbon fiber	mineral fiber	lignin fiber	specification
diameter (μm)	12−14	13−16	12−15	ASTM D2130
length (mm)	2.0−2.5	6.0	1.5−2.0	ASTM D204
tensile strength (MPa)	765−980	2500−3500	100−300	ASTM D2256
surface area (m^2/g)	0.19	0.13	1.8	N/A
density (g/cm^3)	1.3−2.0	2.65−3.05	1.1−1.3	ASTM D3800
melting temperature (°C)	700	1600	<250	ASTM D276
elongation at break (%)	2.1−2.5	3.2	N/A	ASTM D2343

4.2. Experimental Methods. *4.2.1. Preparation of Fiber−Bitumen Binders.* Both modified bitumen and fibers were preheated in an oven at 165 °C for 120 min before blending. To find the stabilization and reinforcement effect of different fibers on the fiber−bitumen binder, 0, 0.1, 0.2, 0.3, 0.4, and 0.5 wt % of fibers were added to the bitumen and mixed homogeneously to prepare fiber−bitumen binders. The concentration of 0 wt % represents the blank bitumen.

During the preparation of samples, 500 g of preheated modified bitumen was added to a 1000 mL barrel and then transferred into an oven. The fiber was added to the modified bitumen slowly with continuous stirring at 600 rpm to avoid the possible agglomeration of the fiber. The mixture was heated and mixed at 170 °C for 120 min to generate a uniform fiber−bitumen binder.

4.2.2. Softening Point T_{r+b} and Penetration Test. The T_{r+b} and the penetration experimental methods have been introduced in our previous manuscripts.[33,34]

The T_{r+b} of the fiber−bitumen binder, in other words, the temperature at which the fiber−bitumen binder changes from solid to liquid, was tested via a WSY-025E fiber−bitumen softening point instrument produced by Wuxi Petroleum Bitumen Apparatus Co. Ltd. according to the Specification ASTM D 36. In this test, a 3.5 g steel ball and a 20 mm steel ring were used. The fiber−bitumen binder was cooled at 5 °C for 15 min and then heated at a rate of 5 °C/min to soften the fiber−bitumen binder until it can allow the ball accommodated in the fiber−bitumen binder with a depth of 25.4 mm.

The penetration is to determine the hardness and viscosity of the fiber−bitumen binder, and it was tested via a WSY-026 penetration instrument produced by Wuxi Petroleum Bitumen Apparatus Co. Ltd. In this test, a container of the fiber−bitumen binder stored at 25 °C was penetrated by a standard 100 g needle with the loading time of 5 s according to the Specification ASTM D5. Penetration is defined as the depth of the needle penetrated in the fiber−bitumen binder, which is expressed in the unit of 0.1 mm.

4.2.3. Mesh-Basket Draindown Experiment. To check the adsorption and stabilization effect of different fibers on the fiber−bitumen binder, the mesh-basket draindown experiment was performed, and the method has been introduced in our previous paper.[33,34] Ten weight percentage of the fiber in the fiber−bitumen binder (approximately 0.3 wt % fiber in the bitumen concrete) was selected based on the pavement engineering practice. Then, 40 g of the above sample was put in a steel mesh basket with a sieve size of 0.25 mm uniformly and kept at room temperature for 120 min. The mesh basket with the sample was transferred to an oven at a higher temperature; as a result, some fiber−bitumen binders melted, flowed, and dropped out. Typically, we set two different temperatures for all the fiber−bitumen binders: 130 °C and 140 °C. It is noted that due to no evident bitumen drainage found at these two temperatures, an extra test temperature at 170 °C was performed for these fiber−bitumen binders. Finally, the weight of the specimen was measured with an interval of 30 min to calculate the loss of the bitumen, and a smaller loss of the bitumen indicates a higher capacity to stabilize and adsorb the bitumen.

4.2.4. Cone Penetration and the Viscosity Test. Cone penetration and viscosity test methods have been introduced in our previous manuscript.[33,34]

Cone penetration of the fiber−bitumen binder was performed to find the fiber−bitumen binder's resistance to flow and shear, and it was carried out via a WSY-026 penetration instrument produced by Wuxi Petroleum Bitumen Apparatus Co. Ltd. Similar to the penetration test introduced in Section 4.2.2, the unit of cone penetration is 0.1 mm as well. The difference is that the cone penetration is the depth of a standard cone with a load of 200 g penetrated into the fiber−bitumen binder. Prior to the test, the fiber−bitumen binder was fully cooled and solidified at room temperature and then placed at room temperature for no less than 60 min in a water bath. Then, the binder was taken out of the water bath and an iron cone was put on its surface. The standard cone slowly penetrated into the fiber−bitumen binder until it stopped sinking. Finally, the penetration depth was recorded. It is noteworthy that the standard cone cannot pierce through the fiber−bitumen binder completely. The viscosity of the fiber−bitumen binder was measured via a DV2TLV rotational viscometer produced by Brookfield Engineering Inc.

4.2.5. Scanning Electron Microscopy (SEM). SEM instrument makes use of a very fine electron beam to detect the surface of the observed specimen. During the scanning process, the electron beam will interact with the sample, and then generate physical information on the sample surface. By collecting, converting, and enlarging the physical information, we can gather information on the surface microstructure and other information on the sample. SEM is an important tool for studying the surface structure of materials. The surface morphology of fiber materials is one of the important factors that affect its function in the fiber−bitumen binder. Hence, three fiber (lignin fiber, carbon fiber, and mineral fiber) microstructures were observed via a Hitachi S-4800 SEM device with an accelerating voltage of 5.0 kV. It is noted that the specimen should be sprayed with gold as a result of the weak conductivity. Several fields were checked at different magnifications to get more information on the prevalent

https://doi.org/10.1021/acsomega.2c05677
ACS Omega 2022, 7, 44207−44214

features to find the surface morphology difference among these fibers.

4.2.6. Rheological Test. In the study, the dynamic rheological properties of the fiber−bitumen binder under a certain temperature and loading frequency were evaluated via a DSR. During the test, a strain-controlling mode is used, and the strain and frequency are 10% and 1.59 Hz, respectively. While measuring the high-temperature performance of the fiber−bitumen binders at 64, 70, 76, and 82 °C, a parallel-plate mold with a diameter of 25 mm is used and the thickness of the fiber−bitumen binder is 1 mm, which in accordance with the Specification AASHTO-TP5. Phase angle δ measured via the DSR experiment reflects the proportion of viscous and elastic components in the fiber−bitumen binder, and a higher δ means a greater proportion of the viscous component in the fiber−bitumen binder, indicating the preference for a permanent deformation at high temperature. Meanwhile, $G^*/\sin\delta$ refers to the rutting factor, which is used as an indicator of the permanent deformation performance of bitumen materials.[35] The higher the rutting factor, the smaller the flow deformation of the fiber−bitumen binder at a high temperature, in other words, the stronger the resistance to rutting deformation.

AUTHOR INFORMATION

Corresponding Author

Jilei Liang − *College of Pharmacy and Chemistry & Chemical Engineering, Taizhou University, Taizhou 225300, P. R. China*; Email: liangjilei_httplan@126.com

Authors

Mengmeng Wu − *College of Pharmacy and Chemistry & Chemical Engineering, Taizhou University, Taizhou 225300, P. R. China*

Hongmei Cai − *Taizhou Customs, Taizhou 225300, P. R. China*

Hao Wang − *College of Pharmacy and Chemistry & Chemical Engineering, Taizhou University, Taizhou 225300, P. R. China*

Jia wei Hua − *College of Pharmacy and Chemistry & Chemical Engineering, Taizhou University, Taizhou 225300, P. R. China*

Yuzhen Zhang − *State Key Laboratory of Heavy Oil Processing, China University of Petroleum (East China), Qingdao 266555, P. R. China*

Complete contact information is available at: https://pubs.acs.org/10.1021/acsomega.2c05677

Notes

The authors declare no competing financial interest.

ACKNOWLEDGMENTS

Financial support from the National Natural Science Foundation of China (22078227), the State Key Laboratory of Heavy Oil Processing (SKLOP201902005), the Qing Lan Project of Jiangsu Province of China, the Natural Science Foundation of Jiangsu Higher Education Institutions of China (22KJB150040), the Science and Technology Support Program (Social Development) of Taizhou (SSF20210021), and the Research Foundation for Talented Scholars of Taizhou University (QD2016007 and QD2016012) is gratefully acknowledged.

REFERENCES

(1) Cheraghian, G.; Wistuba, M. P.; Sajad, K.; Ali, B.; Masoud, A.; Andrew, R. B. Engineered nanocomposites in asphalt binders. *Nanotechnol. Rev.* **2022**, *11*, 1047−1067.

(2) Goshtasp, C.; Michael, P. W. Effect of fumed silica nanoparticles on ultraviolet aging resistance of bitumen. *Nanomaterials* **2021**, *11*, No. 454.

(3) Cheraghian, G.; Wistuba, M. P.; Sajad, K.; Ali, B.; Andrew, R. B. Rheological, physicochemical, and microstructural properties of asphalt binder modified by fumed silica nanoparticles. *Sci. Rep.* **2021**, *11*, No. 11455.

(4) Uomoto, T.; Mutsuyoshi, H.; Katsuki, F.; Misra, S. Use of fiber reinforced polymer composites as reinforcing material for concrete. *J. Mater. Civ. Eng.* **2002**, *14*, 191−209.

(5) Luo, D.; Khater, A.; Yue, Y. C.; et al. The performance of asphalt mixtures modified with lignin fiber and glass fiber: A review. *Constr. Build. Mater.* **2019**, *209*, 377−387.

(6) Chen, J. S.; Lin, K. Y. Mechanism and behavior of bitumen strength reinforcement using fibers. *J. Mater. Sci.* **2005**, *40*, 87−95.

(7) Szabó, L.; Imanishi, S.; Hirose, D.; Tsukegi, T.; Wada, N.; Takahashi, K. Mussel-inspired design of a carbon fiber-cellulosic polymer interface toward engineered biobased carbon fiber reinforced composites. *ACS Omega* **2020**, *5*, 27072.

(8) Shin, Y.; Han, K. S.; Arey, B. W.; Bonheyo, G. T. Cotton fiber based sorbents for treating crude oil spills. *ACS Omega* **2020**, *5*, 13894−13901.

(9) Afroughsabet, V.; Geng, G.; Alexander, G.; et al. The influence of expansive cement on the mechanical, physical, and microstructural properties of hybrid-fiber-reinforced concrete. *Cem. Concr. Compos.* **2019**, *96*, 21−32.

(10) Kiran Kumar, N.; Ravitheja, A. Characteristics of stone matrix asphalt by using natural fibers as additives. *Mater. Today* **2019**, *19*, 397−402.

(11) Liu, Y. Y.; Zhang, Z. Y.; Tan, L. J.; et al. Laboratory evaluation of emulsified asphalt reinforced with glass fiber treated with different methods. *J. Cleaner Prod.* **2020**, *274*, 123116−123125.

(12) Patil, N. V.; Netravali, A. N. Enhancing strength of wool fiber using a soy flour sugar-based "green" cross-linker. *ACS Omega* **2019**, *4*, 5392−5401.

(13) Murugan, K. P.; Balaji, M.; Kar, S. S.; et al. Nano fibrous carbon produced from chromium bearing tannery solid waste as the bitumen modifier. *J. Environ. Manage.* **2020**, *270*, 110882−110890.

(14) Abtahi, S. M.; Sheikhzadeh, M.; Hejazi, S. M. Fiber-reinforced asphalt-concrete: A review. *Constr. Build. Mater.* **2010**, *24*, 871−877.

(15) Crispino, M.; Mariani, E.; Toraldo, E. Assessment of fiber-reinforced bituminous mixtures' compaction temperatures through mastics viscosity tests. *Constr. Build. Mater.* **2013**, *38*, 1031−1039.

(16) Francioso, V.; Moro, C.; Castillo, A.; Velay-Lizancos, M. Effect of elevated temperature on flexural behavior and fibers-matrix bonding of recycled PP fiber-reinforced cementitious composite. *Constr. Build. Mater.* **2020**, No. 121243.

(17) Chen, H. X.; Xu, Q. W. Experimental study of fibers in stabilizing and reinforcing asphalt binder. *Fuel* **2010**, *89*, 1616−1622.

(18) Hassan, H. F.; Oraimi, S. A.; Taha, R. Evaluation of open-graded friction course mixtures containing cellulose fibers and styrene butadiene rubber polymer. *J. Mater. Civ. Eng.* **2005**, *17*, 416−422.

(19) Peltonen, P. Wear and deformation characteristics of fiber reinforced asphalt pavements. *Constr. Build. Mater.* **1991**, *5*, 18−22.

(20) Gao, J.; Guo, H. Y.; Wang, X. F.; et al. Microwave deicing for asphalt mixture containing steel wool fibers. *J. Cleaner Prod.* **2019**, *206*, 1110−1122.

(21) Fritschy, G.; Papirer, E. Dynamic-mechanical properties of a bitumen-silica composite. *Rheol. Acta* **1979**, *18*, 749−755.

(22) Chen, Z. N.; Yi, J. Y.; Chen, Z. G.; Feng, D. Properties of asphalt binder modified by corn stalk fiber. *Constr. Build. Mater.* **2019**, *212*, 225−235.

(23) Arabani, M.; Shabani, A. Evaluation of the ceramic fiber modified asphalt binder. *Constr. Build. Mater.* **2019**, *205*, 377−386.

(24) Morozov, V. A.; Starov, D.; Shakhova, N.; Kolobkov, V. Production of paving asphalts from high-wax crude oils. *Chem. Tech. Fuels Oil* **2004**, *40*, 382−388.
(25) Putman, B. J.; Amirkhanian, S. N. Utilization of waste fibers in stone matrix asphalt mixtures. *Resour., Conserv. Recycl.* **2004**, *42*, 265−274.
(26) Yang, C.; Zhou, F.; Feng, W.; Tian, Z.; Yuan, L.; Gao, L. Plugging mechanism of fibers and particulates in hydraulic fracture. *J. Pet. Sci. Eng.* **2019**, *176*, 396−402.
(27) Li, V. C. Post crack scaling relations for fiber reinforced cementitious composites. *J. Mater. Civ. Eng.* **1992**, *4*, 41−57.
(28) Qin, X.; Shen, A. Q.; Guo, Y. C.; et al. Characterization of asphalt mastics reinforced with basalt fibers. *Constr. Build. Mater.* **2018**, *159*, 508−516.
(29) Chen, H. X.; Xu, Q. W. Experimental study of fibers in stabilizing and reinforcing asphalt binder. *Fuel* **2010**, *89*, 1616−1622.
(30) Chen, J. S.; Peng, C. H. Analyses of tensile failure properties of asphalt-Mineral filler mastics. *J. Mater. Civ. Eng.* **1998**, *10*, 256−262.
(31) Li, P. L.; Jiang, X. M.; Ding, Z.; et al. Analysis of viscosity and composition properties for crumb rubber modified asphalt. *Constr. Build. Mater.* **2018**, *169*, 638−647.
(32) Zhang, L.; Zhou, F.; Feng, W.; Pournik, M.; Li, Z.; Li, X. Experimental study on plugging behavior of degradable fibers andparticulates within acid-etched fracture. *J. Pet. Sci. Eng.* **2020**, *185*, No. 106455.
(33) Wu, M. M.; Li, R.; Zhang, Y. Z.; et al. Reinforcement effect of fiber and deoiled asphalt on high viscosity rubber/SBS modified asphalt mortar. *Pet. Sci.* **2014**, *11*, 454−459.
(34) Wu, M. M.; Li, R.; Zhang, Y. Z.; et al. Stabilizing and reinforcing effects of different fibers on asphalt mortar performance. *Pet. Sci.* **2015**, *12*, 189−196.
(35) Wu, M. M.; Zhao, J.; Cai, H. M.; Liang, J. L.; Qian, S.; Chen, H. L.; Chen, H.; He, Q. M.; He, Q.; Zhang, Y. Z. Effect of fibers on the performance of a porous friction course. *ACS Omega* **2022**, *7*, 28324−28333.

https://doi.org/10.1021/acsomega.2c05677
ACS Omega 2022, 7, 44207−44214